ЖУРНАЛ ВЫСШЕЙ НЕРВНОЙ ДЕЯТЕЛЬНОСТИ, 2020, том 70, № 3, с. 341–350

ФИЗИОЛОГИЧЕСКИЕ МЕХАНИЗМЫ ПОВЕДЕНИЯ ЖИВОТНЫХ: ВОСПРИЯТИЕ ВНЕШНИХ СТИМУЛОВ, ДВИГАТЕЛЬНАЯ АКТИВНОСТЬ, ОБУЧЕНИЕ И ПАМЯТЬ

УДК 611.813.14, 611.81.013

EARLY SHARP WAVE SYNCHRONIZATION ALONG THE SEPTO-TEMPORAL AXIS OF THE NEONATAL RAT HIPPOCAMPUS

© 2020 г. G. Valeeva[a], V. Rychkova[a], D. Vinokurova[a], A. Nasretdinov[a], R. Khazipov[a,b,*]

[a] Laboratory of Neurobiology, Kazan Federal University, Kazan, Russia

[b] Aix-Marseille University, Institut de neurobiologie de la méditerranée, Institut National de la Santé et de la Recherche Médicale, Marseille, France

*e-mail: roustem.khazipov@inserm.fr

Received August 1, 2019; revised August 25, 2019; accepted September 16, 2019

In the neonatal rat hippocampus, the first and predominant pattern of synchronized neuronal network activity is early sharp waves (eSPWs) occurring at a frequency of ~2–4 events per minute. However, how eSPWs are organized longitudinally along the septo-temporal hippocampal axis remains unknown. Using silicone probe recordings from the septal and intermediate segments of the CA1 hippocampus in neonatal rats *in vivo* we found that eSPWs are highly synchronized longitudinally. The amplitudes of eSPWs in the septal and intermediate segments of the hippocampus were also highly correlated. eSPWs also supported longitudinal synchronization of CA1 multiple unit activity. Spatial-temporal analysis revealed a septal-temporal gradient with more frequent initiation of eSPWs in the septal regions. The speed of eSPW longitudinal propagation attained ~250 mm/s. We suggest that longitudinal correlated activity supported by synchronized eSPWs emerges early during postnatal development and may participate in the formation of intrahippocampal connections in the developing hippocampus.

Keywords: hippocampus, neonate, sharp waves, synchronization

DOI: 10.31857/S0044467720030132

Early Sharp Waves (eSPWs) are the earliest pattern of synchronized activity in the developing rodent hippocampus considered as a prototype of SPWs in adults [Karlsson et al., 2006; Leinekugel et al., 2002; Marguet et al., 2015; Mohns et al., 2007; Mohns, Blumberg, 2008; Valeeva et al., 2019a; Buzsaki, 2015]. Similarly to the SPW-ripple complexes in adults [Buzsaki, 2015; Csicsvari et al., 2000; Ylinen et al., 1995], eSPWs are associated with a short-lasting negative local field potential deflection below the CA1 pyramidal cell layer, massive activation of synaptic inputs and collective neuronal discharge in the hippocampal network [Karlsson et al., 2006; Leinekugel et al., 2002; Marguet et al., 2015; Mohns et al., 2007; Mohns, Blumberg, 2008; Valeeva et al., 2019a; Valeeva et al., 2019b]. Yet, despite the similarities in general electrographic phenotype, eSPWs display some unique features different from adult SPWs. For example, eSPWs lack the high-frequency ripple oscillations that are characteristic of adult SPWs [Buhl, Buzsaki, 2005]. Also, eSPWs are reliably triggered by myoclonic movements of neonatal animals, whereas in adults, SPWs, which mainly occur during sleep and periods of immobility, are not associated with movements of the animal [Buzsaki, 2015; Karlsson et al., 2006; Marguet et al., 2015; Valeeva et al., 2019a]. Generation of eSPWs involves activation of entorhinal inputs to the hippocampus suggesting that eSPWs are bottom-up network events embedded into large scale signaling by sensory feedback from neonatal movements [Valeeva et al., 2019a]. In contrast, adult SPWs are a typical top-down signal which is internally generated in the hippocampal network and which enable transfer of the time-compressed replay of neuronal sequences learned during exploration from the hippocampus to the neocortex where memories are consolidated [Buzsaki, 2015; Chrobak, Buzsaki, 1994; Ylinen et al., 1995].

Understanding the network mechanisms and physiological roles of eSPWs in the development of hippocampal networks requires knowledge about the spatiotemporal organization of activity in entire hippocampal system. Previous studies

revealed that eSPWs support remarkably high levels of bilateral interhemispheric synchronization of neuronal activity in the left and right hippocampi [Valeeva et al., 2019b] which is also characteristic of adult SPWs [Suzuki, Smith, 1987; Buzsaki, 1989; Buzsaki, 2015]. Adult SPWs also show high synchrony levels along the longitudinal septo-temporal hippocampal axis [Chrobak, Buzsaki, 1996; Patel et al., 2013]. While each part of the adult hippocampus is able to generate SPW-Ripple complexes that further propagate towards its septal or temporal side at a rate of ~350 mm/s, full SPW propagation along the entire hippocampus is rare and characteristic of large-amplitude SPWs. Small-amplitude SPWs display a more local nature [Patel et al., 2013]. In contrast, spatio-temporal organization of hippocampal activity during eSPWs in neonatal animals along the septo-temporal hippocampal axis remains largely unknown.

The only available knowledge on the septal-temporal organization of activity in the developing hippocampus is based on results obtained using isolated intact hippocampus preparations *in vitro*. Multisite recordings along the septo-temporal axis of the *in toto* neonatal hippocampus preparation revealed that the vast majority of giant depolarizing potentials (GDPs), network activity bursts considered as an *in vitro* analogue of SPWs, are generated in the most septal part and propagate slowly at a speed of 7–10 mm/s towards the temporal end of the hippocampus [Leinekugel et al., 1998]. In keeping with this septal-temporal gradient in GDP propagation, isolated segments of the hippocampus were able to generate GDPs with the highest frequency of generation in the septal segments [Leinekugel et al., 1998]. However, to what extent these septal-temporal gradients and the slow propagation velocity of GDPs in the intact hippocampus *in vitro* are characteristic of eSPWs in rat pups *in vivo* remains unknown.

Here, we addressed the spatio-temporal properties of eSPWs along the longitudinal axis of the hippocampus in neonatal rats *in vivo*. With this aim, we performed field potential and multiple unit recordings from the septal and intermediate hippocampal segments of head-restrained non-anaesthetized neonatal rats using multisite silicone probes.

METHODS

This work was carried out in accordance with EU Directive 2010/63/EU for animal experiments and all animal-use protocols were approved by the French National Institute of Health and Medical Research (INSERM, protocol N007.08.01) and Kazan Federal University on the use of laboratory animals (ethical approval by the Institutional Animal Care and Use Committee of Kazan State Medical University N9-2013).

Wistar rats of either sex from postnatal days (P) 5–7 from in-house breeding colony were used. Preparation of the animals for recordings was performed under deep isoflurane anesthesia the day before recording as previously described [Akhmetshina et al., 2016; Valeeva et al., 2019a]. Recordings were performed from head-restrained non-anesthetized rats. A metal ring was fixed to the skull with dental cement and *via* ball-joint to a magnetic stand. Animals were surrounded by a cotton nest and heated *via* a thermal pad (35–37°C) throughout the recording session.

Extracellular recordings of local field potentials (LFPs) and multiple unit activity (MUA) were performed along the CA1 – dentate gyrus axis of the dorsal and intermediate segments of the hippocampus using a pair of 16-site linear silicon probes with 50 μm separation distance between the electrodes (five animals) or an eight-shank 64-site probe with 200 μm separation distance (one animal; NeuroNexus, Ann Arbor, MI, USA). DiI coated silicone probes were placed using stereotaxic coordinates [Khazipov et al., 2015]: the septal probe and the first shank of the array were located 1.8–1.9 mm AP, and the intermediate probe – 2.3–2.4 mm AP. Eight shanks of the array were inserted parallel with the septo-temporal axis of the hippocampus. Bare 1.5 mm long chlorided silver wire inserted into the occipital or frontal cortex served as a ground electrode. Signals from extracellular recordings were amplified and filtered (10000×; 0.15–10 kHz) using a DigitalLynxSX amplifier (Neuralynx, Bozeman, MT, USA) and digitized at 32 kHz. From 30 min to an hour of spontaneous activity were recorded in each animal.

After recordings the animals were deeply anesthetized with urethane (3 g/kg, intraperitoneally) and perfused intracardially with 4% paraformaldehyde and 1% glutaraldehyde (Sigma). The brains were removed and left for fixation for a few days. One hundred micrometer-thick coronal slices were cut using a Vibratome (Thermo Fisher Scientific, Waltham, MA, USA). Electrode positions were identified from the DiI tracks overlaid on the microphotographs of sections after cresyl violet staining.

Wideband recordings were preprocessed using custom-written functions in MATLAB (MathWorks, Natick, MA, USA). eSPWs were detected semi-automatically from down-sampled (1,000 Hz), bandpass filtered (3–100 Hz, digital RC filter) LFP signals. All events reaching an amplitude greater than 1.5 standard deviations of the filtered LFP on *sl-m* and *pcl* channels (negative and positive peaks, respectively) were first considered as putative eSPWs. To discard movement and static artifacts, LFP segments from –1 s to 1 around the eSPW were visually inspected. The eSPW onset was defined as the time when the first LFP derivative in *sl-m* reached a threshold of 2 mV/s. Raw data were filtered using a 250–4000 Hz bandpass wavelet filter (Daubechies 4) and spikes were detected as negative events exceeding –3.5 standard deviations of the filtered signal. Time lags were calculated from peri-onset time histograms as described previously [Valeeva et al., 2019a].

Statistical analysis was performed using the MATLAB Statistics toolbox. Group comparisons were done using one- and paired-sample Wilcoxon signed-rank tests. *P*-value of less than 0.05 was considered significant. Correlations between variables were estimated using the Spearman (*r*) correlation coefficients. Unless indicated, data are presented as mean ± SD.

RESULTS

Local field potential and multiple unit activity were recorded simultaneously from the septal and intermediate segments of the left hippocampus in six P5–7 neonatal rats. The septal and intermediate recording sites were located in CA1 and spaced apart by a distance of 1.2–2.4 mm along the longitudinal hippocampal axis (fig. 1 (a)). In accordance with previous studies, eSPWs recorded at both sites had similar depth profiles with characteristic current sinks in *s. radiatum* (*sr*) and *s. lacunosum-molecilare* (*sl-m*) and were associated with pronounced neuronal firing in the CA1 pyramidal layer [Valeeva et al., 2019a] (fig. 1 (b)–(d)). We found that about 94 ± 3% of eSPWs co-occurred at septal and intermediate hippocampal segments. eSPWs recorded at septal and intermediate sites also well-correlated in amplitude with an average Spearman's r value of 0.76 ± 0.14 ($n = 6$; $p < 0.001$; fig. 2).

Nearly half of eSPWs (44 ± 11%) occurred largely synchronously in both segments with a time lag between the onsets of LFP negativity during eSPW of ≤3 ms (1.7 ± 0.1 ms average delay of eSPWs in the intermediate segment from the septal segment; $n = 6$ rats; fig. 3). In 32 ± 9% of cases, eSPWs appeared first in the septal segment and propagated to the intermediate segment with a 17.4 ± 4.3 ms delay ($n = 6$). In 24 ± 10% of paired events, eSPWs first emerged in the intermediate segment followed by eSPWs in the septal segment with an 18.2 ± 3.4 ms delay ($n = 6$). Therefore, most frequently eSPWs co-occurred synchronously along the septal/intermediate hippocampal segments, but could also propagate in either the septal-temporal or temporal-septal direction.

We further attempted to estimate the probability of eSPW initiation and speed propagation along the septo-temporal axis (fig. 4). Knowing the stereotaxic coordinates and taking into account the position of the electrodes in serial sections during histological analysis we first calculated electrode position along the hippocampus. A total longitudinal hippocampal length (*L*) of ~7 mm was measured in the hippocampus isolated from age-matched animals. Electrodes in the septal segment were situated at a distance of 1.53 ± 0.08 mm from the most septal end of hippocampus, whereas the electrodes in the intermediate hippocampal segment were situated at distance of 1.78 ± 0.49 mm from the electrodes in the septal segment and at a distance of 3.69 ± 0.56 mm from the most temporal end of hippocampus. On average, 22 ± 1% of the hippocampus was situated septally from the electrodes in the septal segment (distance *A*), 25 ± 7% of the hippocampus was situated between the electrodes (distance *B*), and 53 ± 8% of the hippocampus was temporal to the electrode in the intermediate segment (distance *C*) (fig. 4 (a)). We further assumed that eSPWs can be randomly initiated along the hippocampus and that they fully propagate from the site of initiation septally and temporally along the entire hippocampal length. According to this assumption eSPWs with the shortest delays are presumably initiated in between the electrodes and their percentile estimated as a *B*/*L* fraction (0.25 ± 0.07) of all eSPWs was 30 ± 9% with the delays in a time window of <2 ± 1 ms. The remaining eSPWs were initiated in the more septal part *A* (40 ± 10%) and the more temporal part *C* (30 ± 9%). After correction of these values for the length of parts *A*, *B* and *C*, we further estimated that the probability of eSPW initiation in these parts attained 26 ± 7%/mm, 17 ± 2%/mm, and 8 ± 2%/mm, respectively (fig. 4 (b)). These results suggest a septal-temporal gradient in eSPW initiation that is in keeping with the results ob-

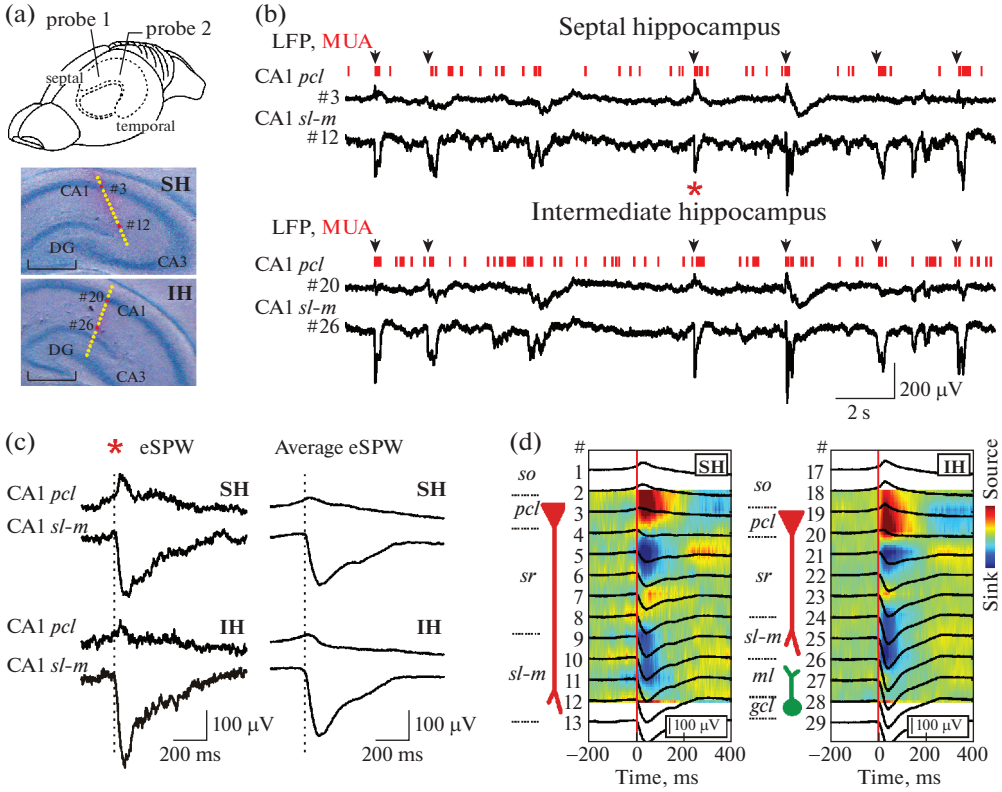

Fig. 1. Co-occurrence of eSPWs in the septal and intermediate hippocampus of neonatal rats. (a) *Top:* A schema of recording probes location in the left hippocampus of a rat pup. *Middle – Bottom:* Recording sites of 16-channel probes overlaid on a cresyl violet stained coronal slices of the septal (SH, middle) and intermediate (IH, bottom) hippocampal segments. Scale bars, 0.5 mm. (b) Simultaneous LFP and MUA recordings from the CA1 pyramidal cell layer (*pcl*, recording sites #3 and #20 on panel (a)) and str. lacunosum-moleculare (*sl-m*, recording sites #12 and #26 on panel (a)) of the septal and intermediate hippocampal segments. Black arrows above the traces indicate eSPWs. (c) The eSPW from panel (b) (red asterisk) and average septal eSPW-triggered LFP in the septal and intermediate hippocampus on an expanded time scale. (d) Septal hippocampal segment eSPWs-triggered LFPs (black) in the septal and intermediate hippocampal segments overlaid on CSD maps.

Рис. 1. Совместная встречаемость ранних острых волн (рОВ) в перегородочном и промежуточном участках гиппокампа новорожденных крыс. (a) *Вверху*: схема расположения регистрирующих электродов в левом гиппокампе новорожденной крысы. *В центре – внизу*: каналы 16-канального регистрирующего электрода, наложенные на микрофотографию окрашенного крезиловым фиолетовым корональных срезов перегородочного (SH, *в центре*) и промежуточного (IH, *внизу*) сегментов гиппокампа. Масштабная линейка соответствует 0.5 мм. (b) Одновременная запись локального полевого потенциала (LFP) и потенциалов действия популяции нейронов (MUA) в CA1 пирамидном слое (*pcl*, каналы регистрации #3 и #20 на панели (a)) и в слое *str. lacunosum-moleculare* (*sl-m*, каналы регистрации #12 и #26 на панели (a)) перегородочного и промежуточного сегментов гиппокампа. Стрелками обозначены рОВ. (c) На развернутой временно́й шкале представлены рОВ, обозначенная на панели (b) красной звездочкой, и усредненный относительно начала рОВ в перегородочном участке локальный полевой потенциал (ЛПП) во время рОВ, зарегистрированных в перегородочном и промежуточном сегментах гиппокампа. (d) ЛПП (черные линии) в перегородочном и промежуточном сегментах гиппокампа, усредненные относительно начала рОВ в перегородочном сегменте и наложенные на карты плотности источников тока.

tained previously in the intact hippocampus *in vitro* [Leinekugel et al., 1998].

We further estimated the speed of eSPW propagation in the septal-temporal and temporal-septal directions from the delays of eSPWs initiated in parts *A* and *C* normalized to the interelectrode distance *B* (fig. 4 (c)). We found that the speed of eSPW propagation in a septal-temporal direction (215 ± 100 mm/s) does not significantly differ from the speed of eSPW propagation in the temporal-septal direction (259 ± 104 mm/s; $p > 0.05$). These values were slightly lower than the speed of SPW propagation in adult animals (~350 mm/s, [Patel et al., 2013]), but much higher than the speed of GDP propagation in the intact hippocampus *in vitro* (~7–10 mm/s, [Leinekugel et al., 1998]).

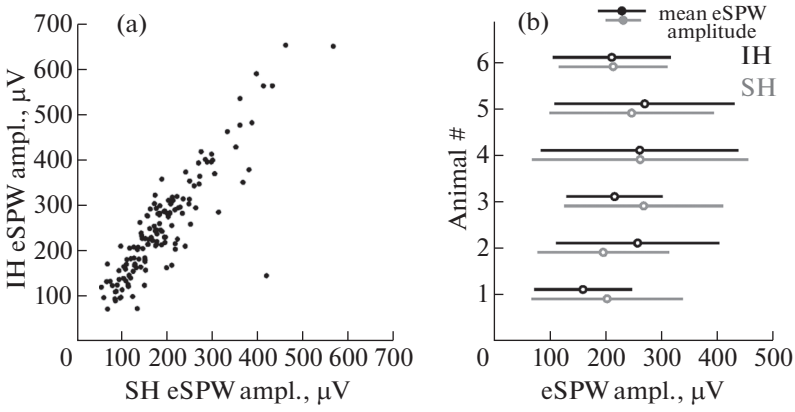

Fig. 2. Relationships between the amplitudes of eSPWs in the septal and intermediate hippocampal segments. (a) Relationships between eSPW amplitudes recorded in CA1 *s-lm* layer of septal and intermediate hippocampal segments of a P6 rat. (b) Amplitude averages of eSPWs in the septal (gray) and intermediate (black) hippocampus of six P5–7 rats (open circles) and group values (closed circles). Error bars show SD.

Рис. 2. Соотношение амплитуд pOB в перегородочном и промежуточном сегментах гиппокампа. (a) Соотношение между амплитудами pOB, зарегистрированными в CA1 *s-lm* слое перегородочного и промежуточного сегментов гиппокампа крысы в возрасте 6 дней после рождения. (b) Средние значения амплитуд pOB в перегородочном (серый) и промежуточном (черный) участках гиппокампа шести крыс в возрасте 5–7 дней после рождения (пустые круглые символы) и групповые данные (заполненные символы). Величина погрешности показана в виде стандартного отклонения.

We also asked whether eSPW amplitude changes during their propagation along the hippocampus. To this aim, we compared the relative amplitudes of eSPWs generated in parts *A* and *C* at the proximal and distant recording sites. In both cases, propagating eSPWs showed a tendency to fade at the more distant site attaining 86 ± 19% of the amplitude at the proximal site in cases of septal-temporal propagation from part *A*, and 82 ± 20% in cases of temporal-septal propagation from part *C*, but this difference was not significant ($p = 0.68$). These results indicate that eSPWs fade little during longitudinal propagation in both directions, at least within the distances explored here.

We performed analysis of MUA associated with eSPWs at the septal and intermediate segments of the hippocampus (fig. 5). Normalized MUA peri-event time histograms (PETHs) triggered by septal eSPW onsets attained maximal values of 6.6 ± 3.3% spikes per ms (6.6 ± 1.3-fold increase above baseline) and 4.7 ± 1.5% spikes per ms (6.7 ± 3.0-fold increase above baseline) with time lags of 72 ± 29 ms and 52 ± 13 ms ($p > 0.05$) in the septal and intermediate segments, respectively. The cross-correlation of MUA between the two recording sites within ± 1 s time window from the eSPW onset revealed no significant longitudinal time lag (–4.0 ± 7.1 ms), while the peak of the cross-correlation attained 2.1 ± 0.8% spikes per ms ($n = 4$ rats; fig. 5 (b)). Thereby, eSPWs supported a high level of longitudinal synchronization of multiple unit activity. Separate MUA analysis during eSPWs originating in portions *A* and *C* failed to reveal a significant time difference of MUA at either of the electrodes, however (not shown), this could be due to a long-lasting increase in MUA through the time course of eSPW relative to the short time lags expected for the rapidly propagating eSPWs.

DISCUSSION

Our main finding is that eSPWs are highly synchronized and support correlated neuronal activity along the septo-temporal hippocampal axis in rat pups *in vivo*. We found that nearly all eSPWs co-occur in the septal and intermediate hippocampal segments. Spatial-temporal analysis of eSPWs suggested that eSPWs are more often initiated in the septal regions of hippocampus than in the temporal regions, which is in keeping with the septal-temporal gradient in the neonatal rat hippocampus previously described in the intact hippocampus *in vitro* [Leinekugel et al., 1998]. This septal-temporal gradient was not observed in adult animals, where the probability of SPW-ripple occurrence is similar along the entire extent of the septo-temporal axis, indicating that each segment of the hippocampus can equally support both SPWs and ripples [Patel et al., 2013] suggesting that the septal-temporal gradient in eSPW ini-

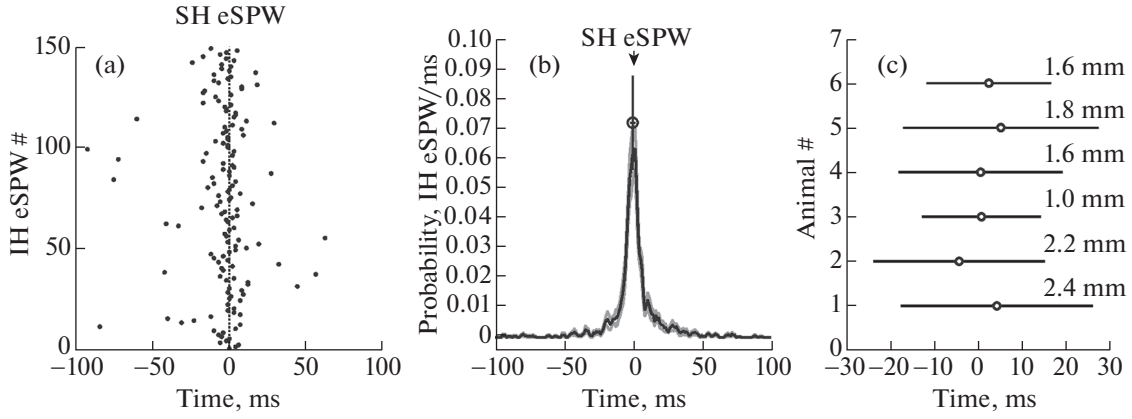

Fig. 3. Temporal relationships between eSPWs recorded in the septal and intermediate hippocampal segments. (a) Septal eSPW onset-triggered raster plot of intermediate eSPW onsets presented for an individual animal. (b) Septal segment eSPW onset-triggered normalized PETH of intermediate eSPW onsets. Group average (open circle; mean ± SD; $n = 6$ animals) show the peak value of normalized PETH and the time lag between septal and intermediate eSPWs. (c) Average time lags between eSPWs in the septal and intermediate hippocampal segments in six P5–7 rats. Error bars show SD. Distance between two recording sites along the septal-temporal hippocampal axis is shown for each animal on the right.

Рис. 3. Временно́е соотношение между рОВ, зарегистрированными в перегородочном и промежуточном сегментах гиппокампа. (а) График распределения времен начала рОВ, возникших в промежуточном участке, относительно времени начала рОВ в перегородочном участке (0 мс) гиппокампа одного из животных. (b) Нормализованная гистограмма распределения времен начала рОВ промежуточного участка относительно времени начала рОВ перегородочного участка гиппокампа (0 мс). Величина группового среднего (обозначено круглым символом; $n = 6$ животных) со стандартным отклонением показывает пиковое значение нормализованной гистограммы и временну́ю задержку между рОВ, регистрируемыми в перегородочном и промежуточном участках гиппокампа. (с) Среднее значение задержки между рОВ в перегородочном и промежуточном сегментах гиппокампа шести крыс в возрасте 5–7 дней после рождения. Величина погрешности показана в виде стандартного отклонения. Справа для каждого животного указано расстояние между двумя участками регистрации вдоль перегородочно-височной оси гиппокампа.

tiation is a developmental phenomenon which is lost during maturation. The slightly lower velocity of the longitudinal eSPW propagation observed in the present study (~250 mm/s) compared to adult SWPs (~350 mm/s) is probably due to a slower axonal conduction velocity in the immature neurons and less developed CA3 recurrent network [Gomez-Di Cesare et al., 1998]. It is conceivable that longitudinal eSPW synchronization in CA1 hippocampus involves the longitudinal recurrent CA3 network which is the origin of adult SPWs [Buzsaki, 2015; Csicsvari et al., 2000; Ylinen et al., 1995], and which is also involved in generation of eSPWs in neonates in both septal and intermediate segments as manifested by a current sink of eSPWs in CA1 *sr* (fig. 1), where CA3-CA1 synapses are located. In addition, longitudinal eSPWs synchronization may also involve synchronous inputs from the entorhinal cortex, which is evidenced by synchronous eSPW current sinks in the septal and intermediate segments in the CA1 *sl-m*, where synapses from the entorhinal cortex are located (fig. 1, see also [Valeeva et al., 2019a]).

While the septal-temporal gradient in eSPW initiation is also characteristic of GDPs in the isolated hippocampus *in vitro,* the speed of GDP propagation is much slower (~7–10 mm/s) [Leinekugel et al., 1998] than that of eSPWs *in vivo* (~250 mm/s). The low speed of GDP propagation has been previously attributed to long and variable delays of spikes evoked by depolarizing GABA, which is importantly involved in generation of GDPs, and to the shunting effects of depolarizing GABA [Valeeva et al., 2010; Khalilov et al., 2015]. In keeping with this, blockade of GABAergic transmission transforms slowly propagating GDPs to fast propagating hypersynchronous, glutamate-driven epileptiform events [Khalilov et al., 1997; Lamsa et al., 2000; Valeeva et al., 2010], which are also evoked by GABA(A) receptor blockade in the neonatal hippocampus *in vivo* [Baram, Snead, 1990]. While the excitatory actions of GABA in the neonatal cortex *in vivo* are debated [Valeeva et al., 2016; Kirmse et al., 2015; Kirmse et al., 2018], these findings suggest that independently of whether GABA exerts depolarizing or hyperpolarizing actions, the roles of

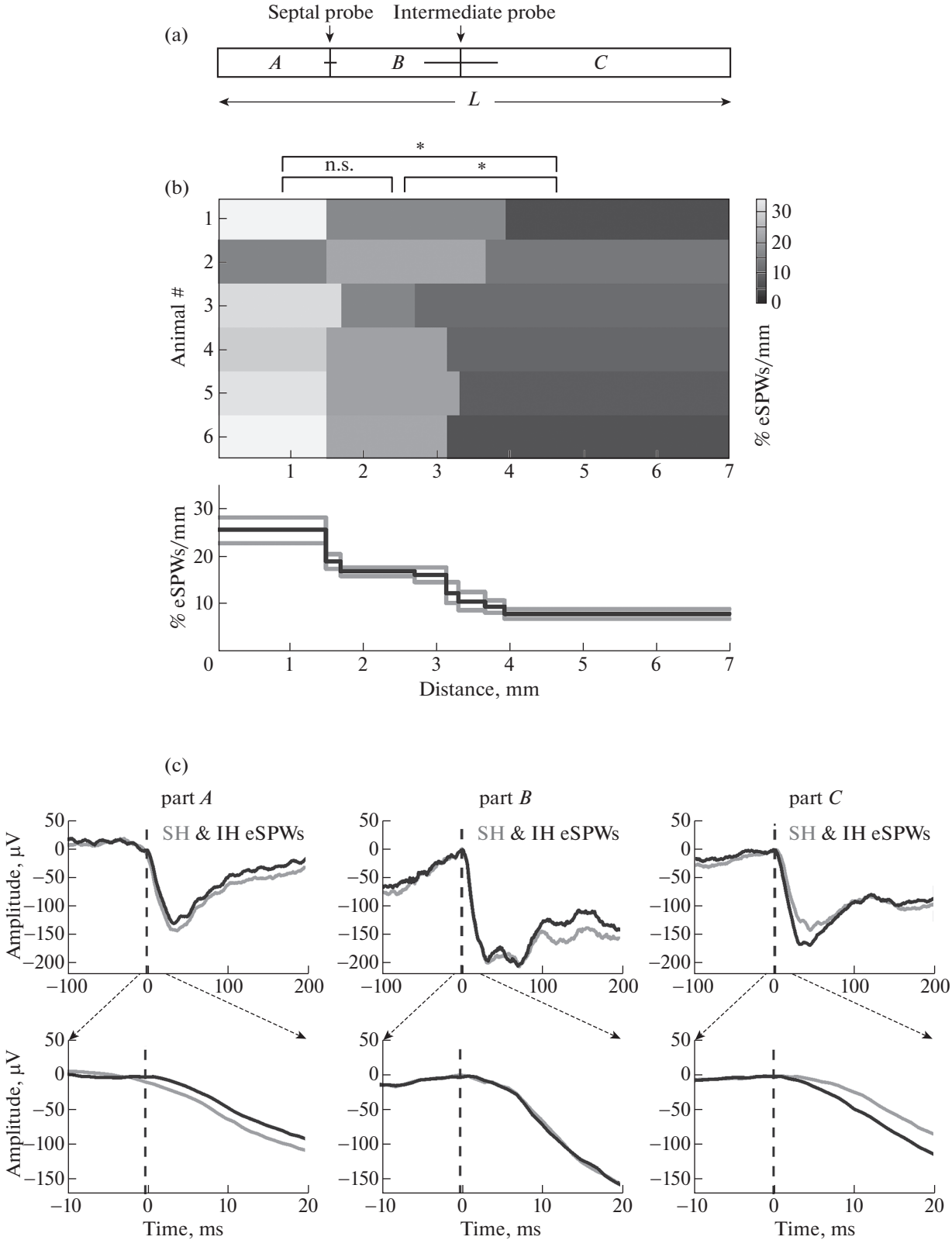

Fig. 4. Estimates of eSPW initiation along the septal-temporal hippocampal axis. (a) A scheme of septal and intermediate probe locations along the septal-temporal hippocampal axis. The arrows point to average coordinate values with horizontal bars showing SD calculated across 6 animals. The probe positions divide the full length of hippocampus (*L*) into three parts: the septal part – distance *A*, distance *B* between the two probes and distance *C*, temporal to the intermediate probe. (b) *Top*, colour coded probability of eSPWs initiation in the parts *A*, *B* and *C* nor-

malized to the length of each part in six P5–7 rats. *Bottom*, average eSPW initiation probability in different parts along the septal-temporal hippocampal axis. Gray lines indicate SE. (c) Example traces of LFP averages in CA1 *sl-m* of septal and intermediate hippocampal segments during eSPWs initiated in parts *A*, *B* and *C*. For each group, LFPs were averaged over 10–50 eSPWs recorded from a P7 rat. Bottom plots show traces around the eSPW onset on an expanded time scale.

Рис. 4. Вероятность возникновения pOB вдоль перегородочно-височной оси гиппокампа. (a) Схема расположения регистрирующих электродов вдоль перегородочно-височной оси гиппокампа. Стрелки указывают на усредненные по 6 животным координаты расположения электродов, горизонтальные линии отражают величину стандартного отклонения. Расположение электродов делит всю длину гиппокампа (*L*) на три участка: перегородочная часть – участок *A*, участок *B* между двумя электродами и участок *C*, простирающийся в височном направлении от электрода промежуточного сегмента. (b) *Вверху:* цветовая карта вероятности возникновения pOB на участках *A*, *B* и *C*, нормализованной к длине каждого участка. Представлены данные по 6 животным в возрасте 5–7 дней после рождения. *Внизу*: средняя вероятность возникновения pOB в различных участках вдоль перегородочно-височной оси гиппокампа. Серые линии отражают величину стандартной ошибки. (c) Примеры усредненного ЛПП в CA1 *sl-m* перегородочного и промежуточного сегментов во время pOB, возникших на участках *A, B* и *C*. Для каждой группы усреднение проводили по 10–50 pOB, зарегистрированным у крысы в возрасте 7 дней после рождения. Нижние графики показывают форму сигнала в области начала pOB на развернутой временно́й шкале.

GABA at the network level remain mainly inhibitory *in vivo* and fast rate of eSPW propagation along the hippocampus mainly involves glutamatergic mechanisms including the CA3 recurrent circuit and synchronous entorhinal input as discussed above.

CONCLUSIONS

In conclusion, we have shown that longitudinal synchronization of activity in the hippocampal system emerges early during postnatal development (it is already present in the electrical activity of several days old rat pups) and that early

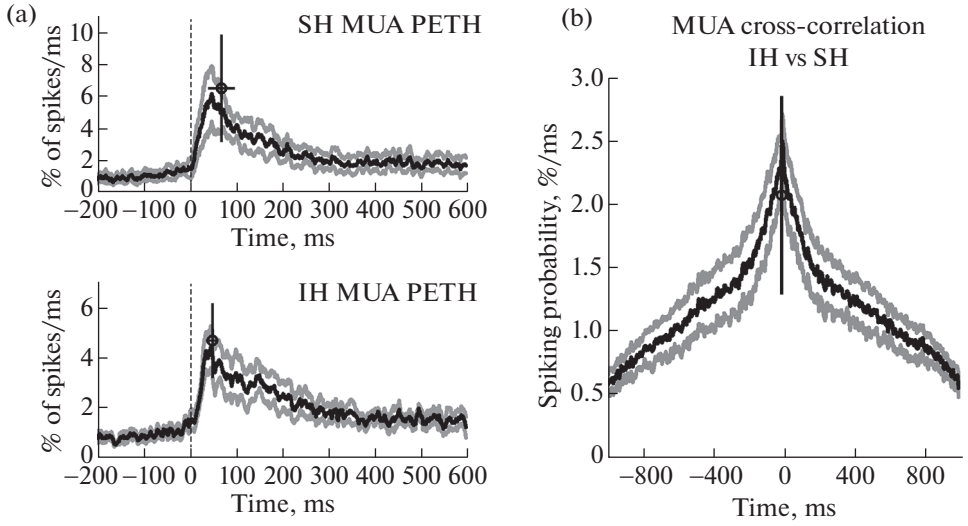

Fig. 5. Longitudinal synchronization of CA1 multiple unit activity during eSPWs. (a) Septal hippocampal segment eSPW onset-triggered MUA PETHs in septal and intermediate hippocampal segments. Average values are shown by open circles, bars show SD. (b) Normalized MUA cross-correlogram in intermediate vs. septal hippocampal segments within the time window of eSPWs. (a), (b): Group averages from 4 animals. Gray lines show standard errors.

Рис. 5. Продольная синхронизация множественных потенциалов действия (ПД) CA1 популяции нейронов во время pOB. (a) Гистограмма распределения времен ПД относительно начала pOB, зарегистрированных в перегородочном сегменте гиппокампа. Среднее значение обозначено круглым символом, в качестве погрешности показано стандартное отклонение. (b) Нормализованная кросс-коррелограмма времен ПД, генерируемых во время pOB в промежуточном сегменте гиппокампа, по отношению к ПД в перегородочном сегменте. (a), (b): Групповые данные по 4 животным. Серые линии показывают величину стандартной ошибки.

longitudinal synchronization is supported by highly correlated eSPWs. Longitudinal synchronization of eSPWs likely contributes to the development of intrahippocampal synaptic connections by means of synchronization of neuronal activity and activity-dependent plasticity. Our results also provide further evidence that eSPWs are a developmental prototype of adult SPWs, which also display a high level of longitudinal synchrony [Patel et al., 2013; Buzsaki, 2015].

FUNDING

This work was supported by the subsidy № 6.2313.2017/4.6 allocated to Kazan Federal University for the state assignment in the sphere of scientific activities, RFBR grant № 17-04-02083 and was performed in the frame of the program of competitive growth of Kazan Federal University and collaborative agreement between the Institut National de la Santé et de la Recherche Médicale and Kazan Federal University (LIA to RK).

REFERENCES

Akhmetshina D., Nasretdinov A., Zakharov A., Valeeva G., Khazipov R. The Nature of the Sensory Input to the Neonatal Rat Barrel Cortex. J. Neurosci. 2016. 36: 9922–9932.

Baram T.Z., Snead O.C. Bicuculline induced seizures in infant rats: ontogeny of behavioral and electrocortical phenomena. Dev. Brain Res. 1990. 57: 291–295.

Buhl D.L., Buzsaki G. Developmental emergence of hippocampal fast-field "ripple" oscillations in the behaving rat pups. Neuroscience. 2005. 134: 1423–1430.

Buzsaki G. Two-stage model of memory trace formation: a role for "noisy" brain states. Neuroscience. 1989. 31: 551–570.

Buzsaki G. Hippocampal sharp wave-ripple: A cognitive biomarker for episodic memory and planning. Hippocampus. 2015. 25: 1073–1188.

Chrobak J.J., Buzsaki G. Selective activation of deep layer (V–VI) retrohippocampal cortical neurons during hippocampal sharp waves in the behaving rat. J. Neurosci. 1994. 14: 6160–6170.

Csicsvari J., Hirase H., Mamiya A., Buzsaki G. Ensemble patterns of hippocampal CA3–CA1 neurons during sharp wave-associated population events. Neuron. 2000. 28: 585–594.

Gomez-Di Cesare C.M., Smith K.L., Rice F.L., Swann J.W. Anatomical properties of fast spiking cells that initiate synchronized population discharges in immature hippocampus. Neuroscience. 1996. 75: 83–97.

Karlsson K.A., Mohns E.J., di Prisco G.V., Blumberg M.S. On the co-occurrence of startles and hippocampal sharp waves in newborn rats. Hippocampus. 2006. 16: 959–965.

Khalilov I., Khazipov R., Esclapez M., Ben-Ari Y. Bicuculline induces ictal seizures in the intact hippocampus recorded *in vitro*. Eur. J. Pharmacol. 1997. 319: R5–R6.

Khalilov I., Minlebaev M., Mukhtarov M., Khazipov R. Dynamic Changes from Depolarizing to Hyperpolarizing GABAergic Actions during Giant Depolarizing Potentials in the Neonatal Rat Hippocampus. J. Neurosci. 2015. 35: 12635–12642.

Khazipov R., Zaynutdinova D., Ogievetsky E., Valeeva G., Mitrukhina O., Manent J.B., Represa A. Atlas of the Postnatal Rat Brain in Stereotaxic Coordinates. Frontiers in Neuroanatomy. 2015. 9: 161. https://doi.org/10.3389/fnana.2015.00161

Kirmse K., Hubner C.A., Isbrandt D., Witte O.W., Holthoff K. GABAergic Transmission during Brain Development: Multiple Effects at Multiple Stages. Neuroscientist. 2018. 24: 36–53.

Kirmse K., Kummer M., Kovalchuk Y., Witte O.W., Garaschuk O., Holthoff K. GABA depolarizes immature neurons and inhibits network activity in the neonatal neocortex *in vivo*. Nat. Commun. 2015. 6: 7750.

Lamsa K., Palva J.M., Ruusuvuori E., Kaila K., Taira T. Synaptic GABA(A) activation inhibits AMPA-kainate receptor-mediated bursting in the newborn (P0-P2) rat hippocampus. J. Neurophysiol. 2000. 83: 359–366.

Leinekugel X., Khalilov I., Ben-Ari Y., Khazipov R. Giant depolarizing potentials: the septal pole of the hippocampus paces the activity of the developing intact septohippocampal complex *in vitro*. Journal of Neuroscience. 1998. 18: 6349–6357.

Leinekugel X., Khazipov R., Cannon R., Hirase H., Ben Ari Y., Buzsaki G. Correlated bursts of activity in the neonatal hippocampus *in vivo*. Science. 2002. 296: 2049–2052.

Marguet S.L., Le-Schulte V.T., Merseburg A., Neu A., Eichler R., Jakovcevski I., Ivanov A., Hanganu-Opatz I.L., Bernard C., Morellini F., Isbrandt D. Treatment during a vulnerable developmental period rescues a genetic epilepsy. Nat. Med. 2015. 21: 1436–1444.

Mohns E.J., Blumberg M.S. Synchronous bursts of neuronal activity in the developing hippocampus: modulation by active sleep and association with emerging gamma and theta rhythms. J. Neurosci. 2008. 28: 10134–10144.

Mohns E.J., Karlsson K.A., Blumberg M.S. Developmental emergence of transient and persistent hippocampal events and oscillations and their associ-

ation with infant seizure susceptibility. Eur. J. Neurosci. 2007. 26: 2719–2730.

Patel J., Schomburg E.W., Berenyi A., Fujisawa S., Buzsaki G. Local generation and propagation of ripples along the septotemporal axis of the hippocampus. J. Neurosci. 2013. 33: 17029–17041.

Suzuki S.S., Smith G.K. Spontaneous EEG spikes in the normal hippocampus. I. Behavioral correlates, laminar profiles and bilateral synchrony. Electroencephalogr. Clin. Neurophysiol. 1987. 67: 348–359.

Valeeva G., Abdullin A., Tyzio R., Skorinkin A., Nikolski E., Ben-Ari Y., Khazipov R. Temporal coding at the immature depolarizing GABAergic synapse. Front Cell Neurosci. 2010. 4.

Valeeva G., Janackova S., Nasretdinov A., Rychkova V., Makarov R., Holmes G.L., Khazipov R., Lenck-Santini P.P. Emergence of Coordinated Activity in the Developing Entorhinal-Hippocampal Network. Cereb. Cortex. 2019a. 29: 906–920.

Valeeva G., Nasretdinov A., Rychkova V., Khazipov R. Bilateral Synchronization of Hippocampal Early Sharp Waves in Neonatal Rats. Front Cell Neurosci. 2019b. 13: 29.

Valeeva G., Tressard T., Mukhtarov M., Baude A., Khazipov R. An Optogenetic Approach for Investigation of Excitatory and Inhibitory Network GABA Actions in Mice Expressing Channelrhodopsin-2 in GABAergic Neurons. J. Neurosci. 2016. 36: 5961–5973.

Ylinen A., Bragin A., Nadasdy Z., Jando G., Szabo I., Sik A., Buzsaki G. Sharp wave associated high-frequency oscillation (200 Hz) in the intact hippocampus: network and intracellular mechanisms. J. Neurosci. 1995. 15: 30–46.

СИНХРОНИЗАЦИЯ РАННИХ ОСТРЫХ ВОЛН ВДОЛЬ ПЕРЕГОРОДОЧНО-ВИСОЧНОЙ ОСИ ГИППОКАМПА НОВОРОЖДЕННЫХ КРЫС

Г. Р. Валеева[1], В. С. Рычкова[1], Д. Е. Винокурова[1], А. Р. Насретдинов[1], Р. Н. Хазипов[1,2,#]

[1]Лаборатория нейробиологии, Казанский федеральный университет, Казань, Россия

[2]Университет Экс-Марсель, Средиземноморский институт нейробиологии, Национальный институт здоровья и медицинских исследований, Марсель, Франция

[#]e-mail: roustem.khazipov@inserm.fr

Ранние острые волны (рОВ) являются первым и преобладающим паттерном синхронизированной сетевой активности нейронов в гиппокампе новорожденных крыс, встречающимся с частотой около 2–4 событий в минуту. Однако остается неизученной продольная организация рОВ вдоль перегородочно-височной (септо-темпоральной) оси гиппокампа. С помощью регистрации активности в перегородочном и промежуточном сегментах CA1 гиппокампа новорожденных крыс *in vivo* мы обнаружили, что рОВ проявляют высокую степень продольной синхронизации. Амплитуда рОВ в перегородочном и промежуточном сегментах тоже имела высокую степень корреляции. Множественные разряды популяции CA1 нейронов во время рОВ также были синхронизированы вдоль длинной оси гиппокампа. Анализ пространственно-временных свойств выявил наличие перегородочно-височного градиента, при котором рОВ чаще возникали в перегородочной области. Скорость продольного распространения рОВ достигала примерно 250 мм/с. Мы предполагаем, что продольная синхронизация активности, обеспечиваемая рОВ, возникает во время раннего постнатального развития и может участвовать в формировании внутренних связей развивающегося гиппокампа.

Ключевые слова: гиппокамп, новорожденный, острые волны, синхронизация